Effects of cobalt on mechanical properties of high silicon ductile irons

R. González-Martínez, J. Sertucha, Jacques Lacaze

Effects of cobalt on mechanical properties of high silicon ductile irons

R. González-Martínez[1], J. Sertucha[1], Jacques Lacaze[2]

1 AZTERLAN, Basque Research and Technology Alliance (BRTA), Durango, Spain

2 CIRIMAT, Université de Toulouse, BP 44362. F-31030 Toulouse, France

Abstract

High silicon ductile irons are being developed due to their advantages relating to pearlitic-ferritic grades (high ductility, fully ferritic structures, good machinability, etc.). Recent studies reported that silicon contents higher than 5.2 wt.% originates drastic embrittlement due to chemical ordering. For improving the mechanical properties, addition of other alloying elements becomes an interesting way of work. This study focuses on the cobalt effect on as-cast microstructures and mechanical properties of ductile irons with silicon contents that maximize ultimate tensile strength. The results obtained show that addition of 4 wt.% cobalt increases the ultimate tensile strength by about 10% and decreases the silicon content at the maximum in this property respecting the unalloyed alloys because cobalt enhances ordering as does silicon.

Keywords: High silicon ductile iron; Cobalt; Microstructure; Mechanical properties.

1. Introduction

In recent years, the new generation of high silicon ductile iron called solution strengthened ferritic ductile irons has attracted great attention of researchers and engineers [1, 2, 3, 4]. High silicon contents improve machinability [5, 6, 7, 8], high-temperature oxidation [9] and corrosion resistance [10, 11], and prevent eutectic carbides formation [12, 13]. High silicon ductile irons with 3.2-4.3 wt.% Si are now included in the European Standard EN 1563:2012. However, it has been previously reported [14] that higher additions of silicon could be also considered, with a maximum ultimate tensile strength value at about 5.2 wt.% Si. At higher silicon contents, the materials become drastically brittle due to chemical ordering of the ferritic matrix. This occurs as in the binary Fe-Si system where the disordered bcc A2 phase (ferrite) becomes B2 (FeSi) and DO_3 (Fe_3Si) ordered at increasing contents of silicon [14]. An additional problem when using high silicon contents is the formation of chunky graphite which has a detrimental effect on mechanical properties [14, 15].

The present study was undertaken with the aim of further improving the mechanical properties of high silicon ductile irons by alloying. Contrary to the so called SiMo ductile iron in which addition of molybdenum leads to precipitation of carbides, the basic idea for high silicon ductile irons is to keep a fully ferritic matrix free of other minor phases. Amongst ferrite promoter elements, aluminium and cobalt have kept relevant interest by researchers. By alloying with 1.21 wt.% Al, a ductile iron with 3.81 wt.% Si, Franzen et al [16] reported an increase of 50 MPa in ultimate tensile stress (UTS) and 80 MPa in yield strength (YS) but with a decrease in elongation at rupture (A) from about 22% to 9%. Cobalt appears of interest as it is a high-melting element and has been reported to increase the nodule count and the ferrite content in ductile irons [17, 18, 19]. In the case of high silicon ductile irons, Weiss et al. [20] also reported a nodularity increase with addition of this element.

Very few reports are available on the effect of cobalt on mechanical properties of ductile irons. Thury et al. [17] made tensile tests on as-cast fully ferritic ductile irons with 2.06-2.24 wt.% Si alloyed with either 0.5 or 1.93 wt.% Co. They reported a small increase in the mechanical properties for the case 1.93 wt.% Co. Mold [18] similarly studied ductile iron alloys with low silicon content (1.5-2.5 wt.%), adding up to 15 wt.% Co. In this case, tensile testing was performed on alloys ferritized by heat-treatment and showed maximum mechanical properties at 6 wt.% Co. Recently, Duwe and Tonn did not find any positive effect of up to 3 wt.% cobalt addition on low temperature toughness of ductile cast iron with 1.6-2.0 wt.% Si [21]. Finally, Fischer et al. [22] studied high

silicon ductile irons with 3.8 and 4.3 wt.% Si and additions of 2 and 4 wt.% Co. They found an increase of UTS and a slight decrease of A with addition of Co.

The aim of the present work is to investigate the effect of cobalt on as-cast microstructures and mechanical properties of alloys with silicon content up to 6 wt.% and to compare the results with those for the corresponding unalloyed alloys [15, 14].

2. Experimental details

A series of 12 ductile irons with silicon content in the range 4-6 wt.% and cobalt content of either 1.4 or 4.0 wt.% were prepared in a medium frequency furnace (250 Hz, 100 kW) 100 kg in capacity. The metallic charges consisted of 20% low alloyed steel scrap and 80% low alloyed pig iron and they were introduced in the furnace crucible together with high purity graphite (>99.0 wt.% carbon) and a FeSi75 alloy (Si = 74.8, Ca = 0.30, Al = 0.76, C = 0.10 and Fe balance, wt.%). Once melting was completed, the composition was adjusted according to the required carbon and silicon contents by adding extra amounts of graphite and of the FeSi75 alloy. At this moment, a new check of the melt composition was made, and the melt temperature was then increased to 1510–1520ºC. Nodularisation treatment was performed following the so-called sandwich method by transferring 50 kg of the prepared alloy to a ladle in which chamber a FeSiMg alloy (grain size 5–25 mm, Si = 46.60, Mg = 6.00, Ca = 0.96, Al = 0.71 and rare earth RE = 0.92, Fe balance, wt.%) were positioned in an amount of 0.6 kg (1.2 wt.% of the batch weight) and then covered with steel scrap (grain size 5–15 mm). After completion of the reaction, the alloy was skimmed and then cast in the moulds. Additions of 2.0–2.5 g Sb was made in the melting furnace to some of the batches (0.004–0.005 wt.% of the batch weight) in order to limit spheroidal graphite degeneracy associated with high silicon contents.

The castings produced were standard Y2 keel-blocks (EN 1563) which were manufactured with chemical bonded sand moulds. Inoculation process was performed by adding 14 g (0.20 wt.% of the total weight of the alloy poured in the mould) of a commercial inoculant (grain size 0.2–0.5 mm, Si = 69.9, Al = 0.93, Ca = 1.38, Bi = 0.49, RE = 0.37 and Fe balance, wt.%) in the mould cavity before pouring it.

After removing the keel-blocks from the moulds, they were cleaned, and several test samples were machined out from their bottom area to avoid the presence of shrinkage porosities and/or inclusions. Both a cylindrical specimen with 10 mm gauge diameter for tensile testing and a parallelepiped sample for hardness measurements were obtained from this area. The tensile parameters, ultimate

tensile strength (UTS), yield strength (YS) and elongation (A), were measured using a Zwick Z250 tensile testing equipment at a controlled strain rate of 0.90 mm/min in the range where YS was determined. This rate was then increased to 24.12 mm/min to determine UTS and A, according to the standard ISO 6892-1, method A224. Brinell hardness (HBW) was measured with an Instron Wolpert apparatus with a 10 mm diameter sphere, a load of 3000 kg and a dwell time of 10 s.

Once tensile testing was completed, one piece of the tensile specimens was used for chemical analysis and to perform the metallographic characterizations. Carbon and sulphur contents were measured by combustion analysis (LECO CS300) while the rest of analysed elements were determined by the ICP-MS technique (Agilent 7500ce) after dissolving a metallic sample in a mixture of acids. The results obtained from these analyses are shown in table 1 where two different carbon equivalent values are included according to Castro et al. [23] and the ASM handbook [24].

Table 1 – Chemical composition (wt.%) of the alloys prepared in this work.

Alloy	C	Si	Co	Mn	P	S	Cu	Cr	Ni	Ti	Mg	Ce	La	Sb	CE*	CE**
1	3.17	3.99	1.31	0.14	<0.015	0.008	<0.02	0.030	0.030	<0.005	0.030	0.0053	0.0028	<0.0005	4.29	4.41
2	3.08	4.47	1.31	0.14	<0.015	0.007	<0.02	0.040	0.030	0.005	0.031	0.0026	0.0029	<0.0005	4.34	4.47
3	2.87	4.74	1.42	0.16	0.014	<0.005	0.022	0.024	0.033	0.012	0.038	0.0063	0.0032	<0.0005	4.20	4.34
4	2.59	5.54	1.44	0.19	0.014	0.006	0.023	0.030	0.038	0.012	0.035	0.0062	0.0032	<0.0005	4.15	4.31
5	2.52	5.95	1.43	0.20	0.010	0.006	0.022	0.034	0.038	0.010	0.036	0.0065	0.0033	<0.0005	4.19	4.37
6	3.09	4.39	3.94	0.19	<0.01	0.010	0.020	0.033	0.038	0.007	0.037	0.0064	0.0031	<0.0007	4.33	4.49
7	3.07	4.20	3.90	0.20	<0.01	0.010	0.020	0.037	0.040	0.007	0.031	0.0053	0.0027	0.0049	4.25	4.41
8	3.05	4.36	4.20	0.20	0.011	0.005	<0.020	0.034	0.046	0.010	0.040	0.0070	0.0036	0.0053	4.28	4.40
9	2.94	4.83	4.13	0.22	0.011	0.005	0.021	0.042	0.048	0.011	0.032	0.0058	0.0028	0.0059	4.30	4.44
10	2.87	5.10	4.22	0.23	0.010	0.006	0.021	0.048	0.052	0.011	0.041	0.0068	0.0034	0.0056	4.30	4.45
11	2.65	5.89	4.40	0.23	<0.010	<0.005	0.020	0.051	0.053	0.012	0.044	0.0072	0.0035	0.0064	4.31	4.48
12	3.14	3.89	4.38	0.20	0.011	0.005	<0.020	0.041	0.048	0.010	0.041	0.0065	0.0033	0.0050	4.24	4.35

*CE = C + 0.28·Si + 0.007·Mn + 0.092·Cu + 0.303·P [23].
**CE = C + 0.31·Si – 0.027·Mn + 0.076·Cu + 0.33·P + 0.40·S [24].

The surfaces where metallographic studies were performed were selected close to the rupture surface of the tensile specimens. After polishing these surfaces, three representative pictures at 100x magnification (0.757 mm^2 each) were obtained per sample without etching so as to determine the fractions of the different graphite shapes using an image analysis software. For this analysis, only graphite particles with an area equal to or higher than 15 μm^2 were considered. Classification of graphite particles was carried out taking into account circularity and the ratio of the minimum to the maximum Feret diameters [25]. The circularity was defined here as the area of a given graphite particle divided by the area of the circle whose diameter is the maximum Feret diameter of the particle. Finally, the particles were sorted in three classes using the criteria shown in table 2. Those

particles that could not be assigned to one of these classes by means of image analysis were then visually classified. As previously [15], chunky graphite (CHG) particles were assigned to class III. The number and area of particles in each class were used for determining the count fractions (f_{CHG}^{count}, f_{V}^{count} and f_{VI}^{count}) and area fractions (f_{CHG}^{A}, f_{V}^{A} and f_{VI}^{A}) respectively. The results listed in table 3 correspond to the average of the values determined from the three metallographic fields. The nodule count values were thus determined from both the count of particles belonging to classes V and VI, N_{V+VI}, or only to class VI, N_{VI}.

Table 2 – Criteria used for the classification of graphite particles.

Class	Circularity	Height-width Feret ratio
III	0.00–0.60	2.0–1000
V	0.50–0.77	1.0–1.5
VI	0.77–1.00	1.0–1.5

The morphology of fracture surfaces was analysed on the remaining piece of the tensile specimens by field-emission scanning electron microscopy (FE-SEM) using a Zeiss Ultra Plus microscope in backscattered electron (BSE) and secondary electron (SE) imaging modes operated at 20 kV.

3. Results

Examples of the graphite particles obtained in the alloys without and with Sb additions are illustrated in figures 1 and 2 respectively. Figure 1a shows the microstructure of alloy #1 with 3.99 wt.% Si and 1.31 wt.% Co while figure 1b shows the microstructure of alloy #5 with an increased silicon content (5.95 wt.%) and a comparable cobalt content (1.43 wt.%). The comparison of these two images confirms that CHG formation increases with the silicon content as already reported [15, 26, 27].

As it is shown in table 1, antimony was added to alloys from #7 to #12 to counteract the formation of CHG. Figures 2a and 2b show the graphite particles distribution in, respectively, alloy #12 (3.89 wt.% Si, 4.38 wt.% Co and 0.0050 wt.% Sb) and alloy #11 (5.89 wt.% Si, 4.40 wt.% Co and 0.0064 wt.% Sb). As for figure 1, these two alloys contain similar cobalt contents with an increased silicon content in the latter one. When comparing the two micrographs of figure 2, it is observed that CHG is almost inexistent due to the beneficial effect of antimony and only a small number of worm-like graphite particles is present in alloy #11 (figure 2b) with the highest silicon content.

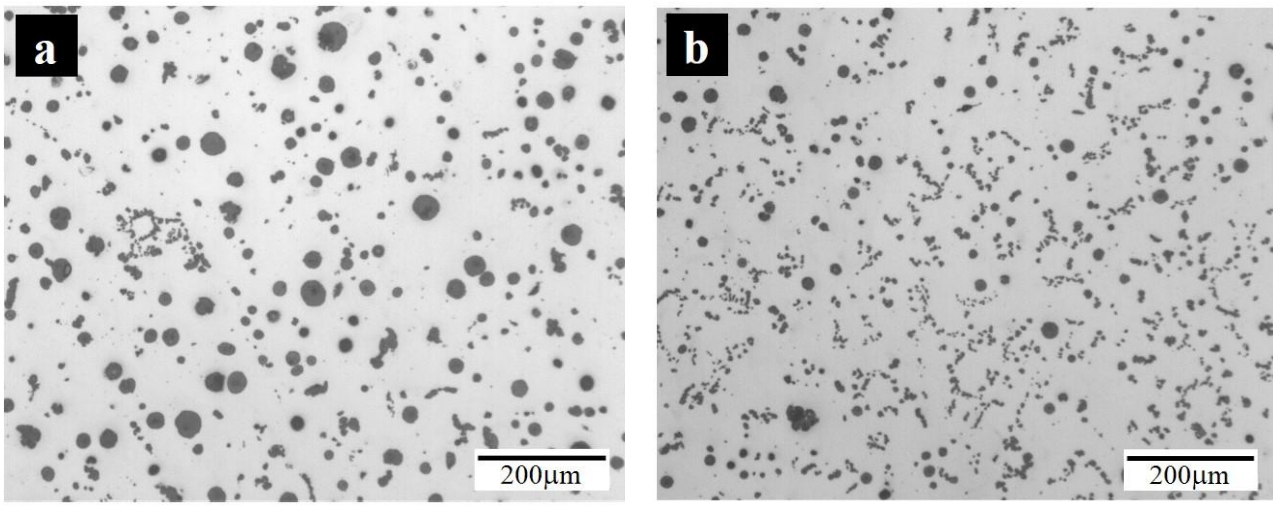

Figure 1 – Graphite morphology of a) alloy #1 (3.99 wt.% Si and 1.31wt.% Co) and b) alloy #5 (5.95 wt.% Si and 1.43 wt.% Co).

The microstructure of all the alloys included in table 1 was ferritic with the presence of a very low amount of small silicon-bearing carbides that were already reported in previous work [14].

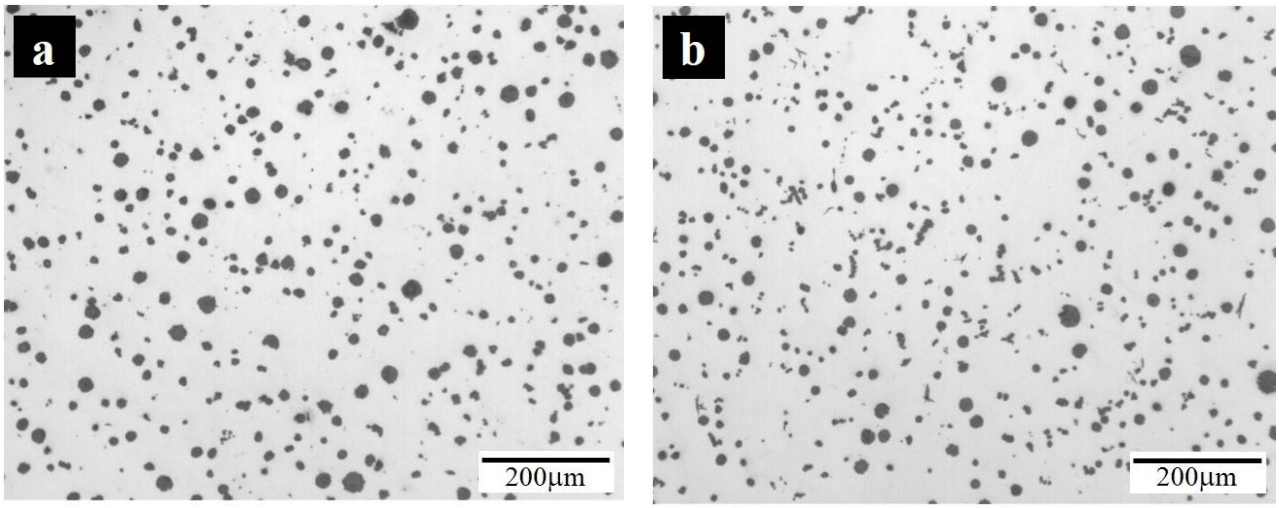

Figure 2 – Optical micrograph of a) alloy #12 (3.89 wt.% Si, 4.38 wt.% Co and 0.0050 wt.%) and b) alloy #11 (5.89 wt.% Si, 4.40 wt.% Co and 0.0064 wt.%).

Nodule count values and the count and area fractions of each graphite class are reported in table 3. Owing to the varying amount of CHG, any effect of the cobalt content on the nodule count was looked for by considering the change of the nodule count over an unit area devoid of chunky graphite. An estimate of this normalized nodule count is given by $N_{V+VI}/(1-f^{A}_{CHG})$ and has been plotted in figure 3a. It may be seen that the normalized nodule count shows a very slight increase with cobalt content in agreement with previous reports [17, 18, 19].

Table 3 – Microstructure data obtained from the ductile irons prepared in the present work.

Alloy	N_{III} (mm^{-2})	N_V (mm^{-2})	N_{VI} (mm^{-2})	N_{V+VI} (mm^{-2})	f_{CHG}^{count}	f_V^{count}	f_{VI}^{count}	f_{CHG}^{A}	f_V^A	f_{VI}^A
1	35	98	278	376	0.09	0.24	0.68	0.13	0.24	0.63
2	134	87	210	296	0.29	0.20	0.50	0.28	0.21	0.51
3	12	80	305	385	0.03	0.20	0.77	0.04	0.18	0.78
4	69	81	258	340	0.16	0.20	0.64	0.19	0.19	0.62
5	809	9	87	95	0.88	0.01	0.10	0.79	0.02	0.19
6	287	68	217	285	0.48	0.12	0.39	0.35	0.16	0.49
7	26	77	309	386	0.06	0.19	0.75	0.09	0.23	0.68
8	5	62	345	406	0.01	0.15	0.84	0.02	0.16	0.82
9	10	81	358	439	0.02	0.18	0.79	0.04	0.21	0.76
10	26	87	337	424	0.06	0.19	0.75	0.06	0.20	0.75
11	90	69	401	470	0.16	0.12	0.71	0.16	0.12	0.72
12	36	59	390	449	0.07	0.12	0.81	0.10	0.14	0.76

As it has been reported previously [14, 15, 28], the amount of CHG increases with silicon content, but other elements like cerium also increase this graphite degeneration which effect can be counteracted by adding controlled amounts of antimony. It was also found that high magnesium contents promote the formation of CHG. For rationalizing the interactions between these three elements, the index Ω_{Si} [28] was developed as follows:

$$\Omega_{Si} = w_{Si} + 800 \cdot \left(w_{Ce} \cdot \frac{55}{140.1} - 2 \cdot w_{Sb} \cdot \frac{55}{121.8} \right) + 50 \cdot w_{Mg} \cdot \frac{55}{24.3}$$

in which w_i is the content in element i (wt.%).

The measured area fraction of CHG is reported as function of Ω_{Si} in figure 3b with solid or open circles depending on whether Sb addition was made or not to the alloy. These data are also compared to values previously reported for alloys with silicon content varying between 3 and 6 wt.% [15]. It is seen that the amount of CHG increases dramatically when Ω_{Si} is over a critical value that was set to Ω_{Si}=7 wt.% for Y2 blocks in the previous works [15, 28]. The addition of cobalt appears to decrease this critical value to about Ω_{Si}=5 wt.%, i.e. to increase the risk of CHG formation. It is interesting that cobalt thus have an effect that appears similar to the known effect of silicon [15, 26, 27, 28] and nickel [29, 30].

Table 4 lists the results of the tensile tests and Brinell hardness measurements together with the relevant amounts of significant elements (Si, Co and Sb) and the CHG area fraction for all the alloys investigated in the present work. It is seen that the four alloys with silicon content higher than

4.83 wt.% were so brittle that UTS could be recorded but was obtained at a strain below 0.2%. Accordingly, no YS and A values are reported for these alloys. The brittle behaviour thus occurs at lower Si content than the 5.2 wt.% reported for alloys without cobalt [14], this will be further detailed below.

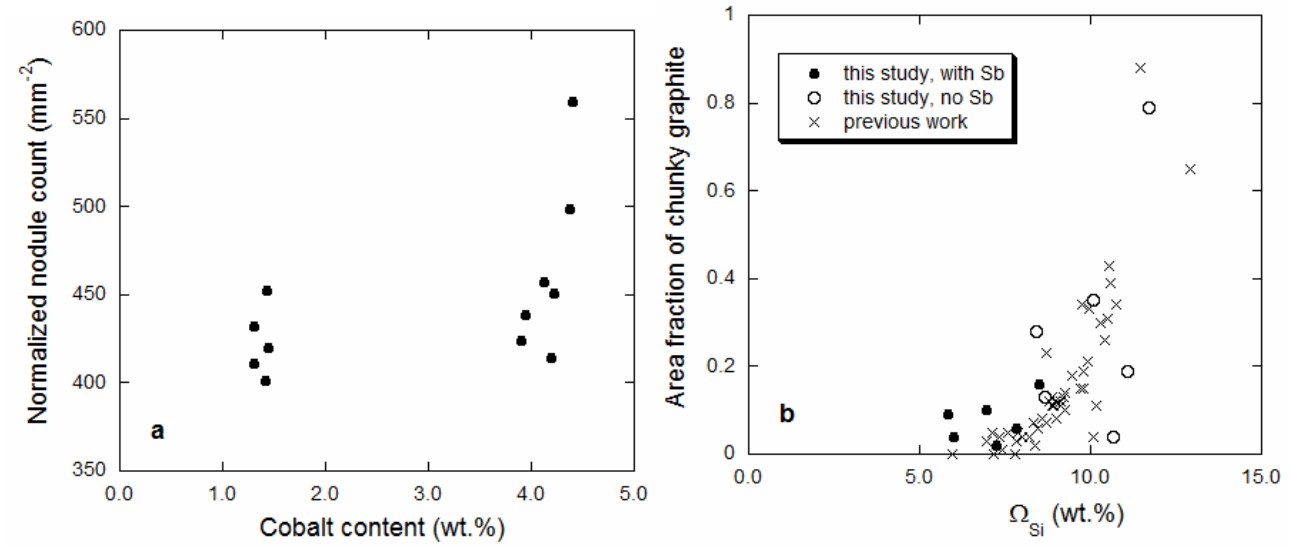

Figure 3 – a) Evolution of the normalized nodule count with cobalt content; b) change in CHG area fraction with Ω_{Si} for Y2 blocks.

Table 4 – Tensile test results (UTS, YS and A), hardness values (HBW), and silicon, antimony and chunky graphite contents in the 12 investigated alloys.

Alloy	UTS (MPa)	YS (MPa)	A (%)	HBW	Si (wt.%)	Co (wt.%)	Sb (wt.%)	f_{CHG}^{A}
1	560	439	15.5	205	3.99	1.31	<0.0005	0.13
2	619	483	9.6	224	4.47	1.31	<0.0005	0.28
3	651	535	3.0	244	4.74	1.42	<0.0005	0.04
4	433	----	---	280	5.54	1.44	<0.0005	0.19
5	184	----	---	306	5.95	1.43	<0.0005	0.79
6	622	499	2.9	228	4.39	3.94	<0.0007	0.35
7	653	486	16.4	225	4.20	3.90	0.0049	0.09
8	638	510	3.0	234	4.36	4.20	0.0053	0.02
9	618	558	0.7	260	4.83	4.13	0.0059	0.04
10	537	-----	----	273	5.10	4.22	0.0056	0.06
11	61	-----	----	310	5.89	4.40	0.0064	0.16
12	610	465	18.4	214	3.89	4.38	0.0050	0.10

Before going into the detail of the effect of cobalt on the mechanical properties, it is worth plotting UTS as function of the area of chunky graphite as done in figure 4. It is seen that the three lowest UTS values appear essentially related to high silicon contents, i.e. when the matrix is so brittle that rupture occurs at elongation less than 0.2%. Focusing on the results at UTS values higher than 450 MPa, it is seen that the amount of chunky graphite may have only a marginal effect, if any. This is in line with previous conclusion that chunky graphite negatively affects the tensile properties of low-silicon (2-3 wt%) ductile irons and not that of high silicon (>3.5 wt.%) ductile irons [14].

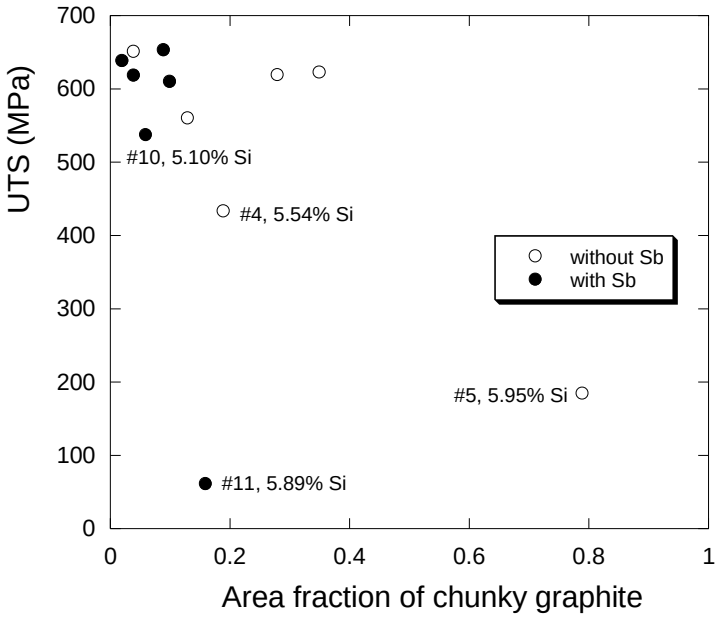

Figure 4 – Area fraction of chunky graphite versus UTS for alloys with and without Sb added. The four alloys with the highest silicon contents are indicated.

In the high silicon ductile irons domain and in agreement with previous reports, a prominent feature of the present study is the high sensitivity of the elongation at rupture with the silicon content. This is illustrated in figure 5 with the strain-stress curves of the four alloys with about 4 wt.% Co added. It is seen that the decrease of the silicon content from 4.83 to 3.89 wt.% leads to a dramatic increase of the elongation at rupture. When the silicon content decreases from 4.83 to 4.36 wt.%, the UTS value increases because the elongation at rupture does so. Further decrease of the silicon content leads to a marked increase in elongation at rupture which is associated to a continuous softening of the matrix. Accordingly, the UTS values passes through a maximum at a silicon content in between 4.20 and 4.36 wt.%. This maximum is thus located at much lower silicon content than the 5.2 wt.% value previously reported for alloys without cobalt added [14].

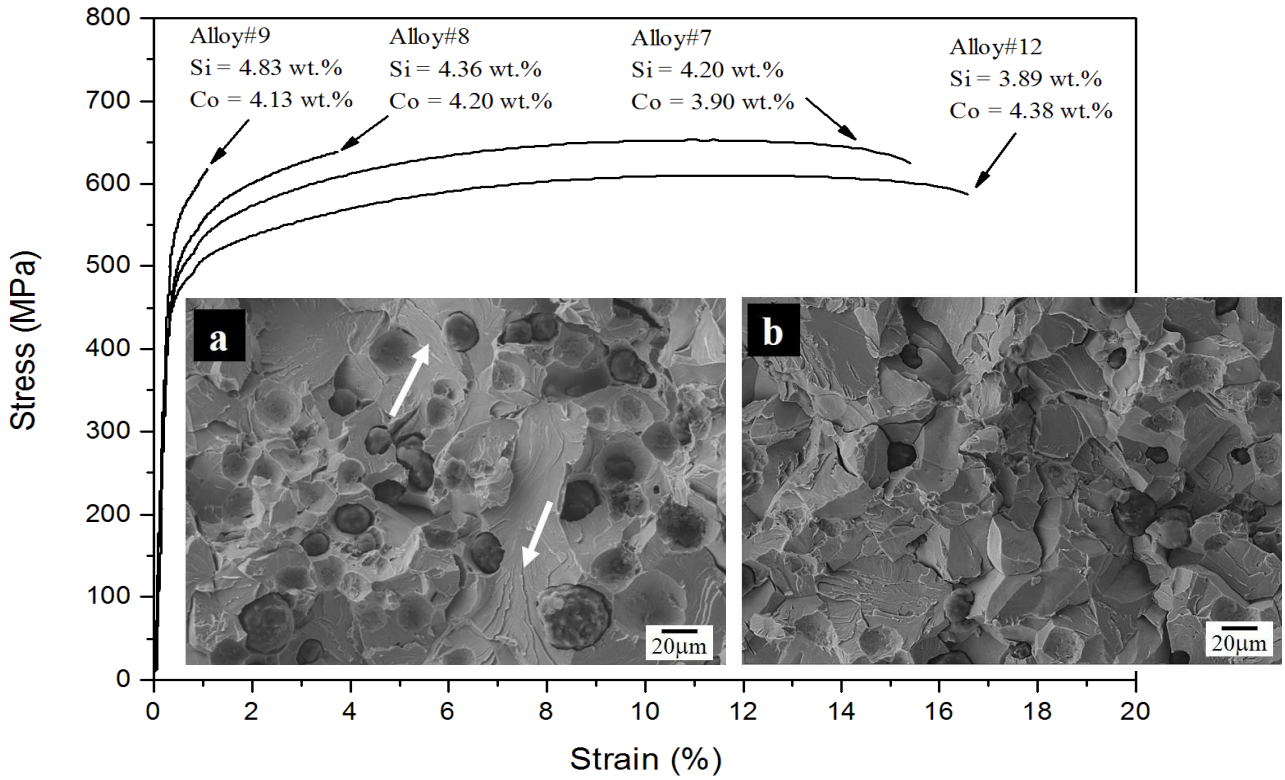

Figure 5 – Stress-strain curves of the high silicon alloys with about 4 wt.% Co and SEM micrograph of the rupture surface of alloys #7 (a) and #8 (b).

SEM characterizations on the rupture surfaces of all samples were carried out. The micrographs inserted in figure 5 illustrate that alloy #7 (micrograph a) showed a ductile rupture with some cleavage facets indicated with the two white arrows while alloy #8 showed essentially a brittle-like fracture with some intergranular cracks (micrograph b).

4. Discussion

This discussion is dedicated at describing the effect of cobalt addition on the relation between silicon content and room temperature mechanical properties of ductile cast irons. In the present work, focus was put on the high silicon range (> 4 wt.%) where a maximum in UTS and YS values was observed [14]. In this domain, no effect of chunky graphite was observed in agreement with figure 4 above.

In figure 6, UTS, YS and HB values are plotted as a function of the silicon content. In this figure, open symbols have been used for the previous results without cobalt addition [14, 15, 31, 32] while solid symbols denote the results from the present work. Among this last group, alloys with about 1.4 wt.% Co are represented with grey symbols while those with 4 wt.% Co are represented with black symbols. It is seen that addition of about 4 wt.% Co slightly increases the HBW values with

respect to the series without cobalt while an addition of 1.4 wt.% does not affect it. However, whatever the addition of cobalt, the YS values seem unchanged with respect to the alloys without cobalt. Looking at the UTS values, it appears that the maximum at 5.2 wt.% Si in the Co-free series (vertical interrupted line) seems to be shifted to about 4.2-4.3 wt.% Si with addition of 4 wt.% cobalt as noticed above in the discussion of figure 5. Considering only the alloys close to this maximum, it is worth mentioning that the addition of 4wt. % Co leads to an increase of 5–10% of the UTS. In contrast, addition of only 1.4 wt.% Co has no effect on UTS.

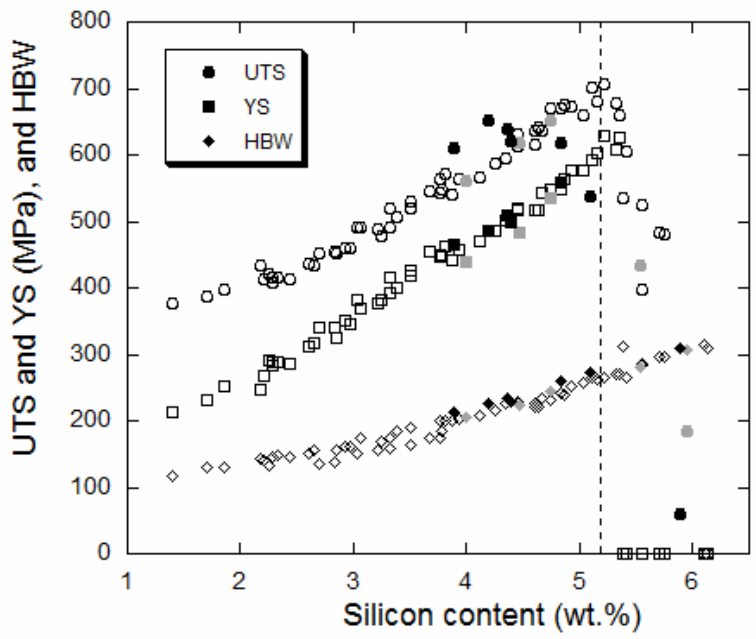

Figure 6 – Comparison of UTS, YS and HBW values from the present work with previous results [14]. The grey symbols are for the alloys with 1.31-1.43 wt.% Co and the black solid symbols correspond to the alloys with 3.94-4.38 wt.% Co content, while open symbols are from previous work [14].

In figure 7, the values of A for the present results (grey solid symbols for alloys with about 1.4 wt.% Co and black ones for those with about 4 wt.% Co) and previous results with no cobalt [14] (open symbols) are plotted against the silicon content. It is seen that A starts decreasing at about 2.5 wt.% Si and is zero 5.3 wt.% Si. This drop has been shown to be due to progressive ordering of the ferritic matrix [14, 33]. The transition between ductile and brittle behaviour may be set at A = 12.5% which corresponds to about 3.85–4.50 wt.% Si whatever the cobalt content is. It is interesting to note that the values for the Co-bearing alloys are above those for the Co-free alloys below this critical limit, while the reverse is true above this limit, which means the drop becomes sharper when increasing the cobalt content.

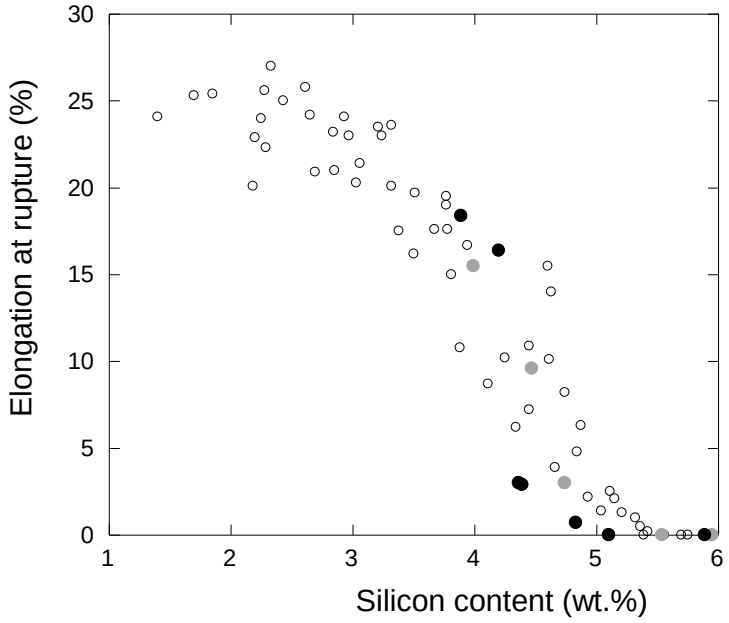

Figure 7 – Evolution of the elongation at rupture A with silicon content. The greyed solid circles are for the alloys with about 1.4 wt.% Co and the black solid circles correspond to the alloys with about 4 wt.% Co, while open symbols correspond to results from a previous work without cobalt [14].

To get some support to the present results, literature data was collected concerning the UTS values. Works by Thury et al. [17], Mold [18] and Fischer et al. [22] could be found which are shortly presented in annex A. Relevant values from these works have then been added to the present and previous results [14] in figure 8 which shows the change of UTS with silicon content. The values obtained from Mold for low silicon alloys with 2-6 wt.% Co are 5-10% higher than the values for alloys without cobalt while the results from Thury et al. do not show any effect of the addition of 2 wt.% of cobalt. Results for high silicon ductile irons from Fischer et al. are in excellent agreement with the present results and show that 4 wt.% Co increase UTS by up to 10% for silicon content in the range of 4.0 to 4.5 wt.%.

The results by Mold and those for high silicon ductile irons thus suggest that addition of 4 wt.% Co leads to an increase by about 10% of the UTS whatever the silicon content. The drop of the UTS value for Co-bearing alloys above 4.4-4.5 wt.% Si in figure 8 may thus be seen as indicating a maximum has been reached at 4.3-4.4 wt.% Si. Such a maximum should be similar to the maximum seen at 5.2 wt.% Si for alloys without cobalt which was indicated with a vertical interrupted line in figure 6. In the previous work on alloys without cobalt [14], this maximum has been associated with the decrease of the elongation at rupture due to the embrittlement effect of silicon addition. Figures 7 and 8 show the same phenomenon occurs here in Co-bearing alloys but at much lower silicon contents.

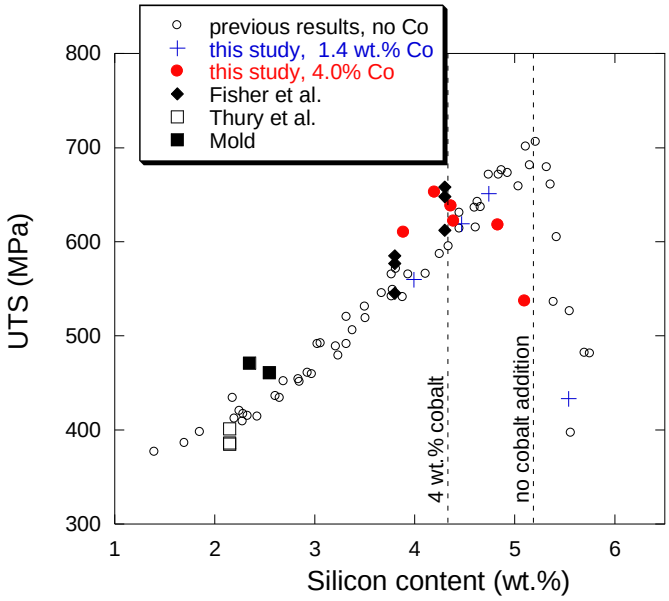

Figure 8 – Comparison of the evolution of UTS values with silicon content from the present work with previous results [14], Thury et al. [17], Mold [18] and Fischer et al. [22]. The vertical interrupted lines indicate the locus of the UTS maximum without (line to the right) or with (line to the left) addition of 4 wt.% Co.

As a matter of fact, works on Fe-Co-Si alloys [34] have shown that cobalt moves the transition between disordered A2 to ordered B2 bcc-ferrite to lower silicon contents. According to the review by Raghavan [35], this decrease amounts to about 0.2 wt.% Si by percent of cobalt added. For a cobalt addition of 4 wt.%, the transition should be shifted by 0.8 wt.% which is exactly the difference seen in figure 8 between the two maxima which are located with the interrupted vertical lines.

5. Conclusion

The strengthening effect of cobalt which was expected from the few literature data available could effectively be observed in the present investigation. The main conclusions obtained are the following:

1. It has been observed that cobalt addition to ductile cast irons with silicon contents in the range 3.89-5.95 wt.% preserved fully ferritic structures in all alloys and slightly increased nodule count only at the highest cobalt addition of about 4 wt.%. Cobalt increases the risk of chunky graphite formation, but this has no effect on the mechanical properties at the high silicon contents considered.

2. An increase by about 10% of the UTS value for a 4 wt.% addition of cobalt has been observed for silicon contents from 3.89 wt.% to about 4.4 wt.%.
3. However, the optimum value of silicon - i.e. the one leading to the maximum UTS value - is strongly decreased with cobalt addition. This is due to the fact that cobalt and silicon both lead to chemical ordering of the ferritic matrix, and their effect is additive when present together.
4. Consequently, addition of cobalt does not appear of interest as the 10% increase of UTS may be achieved with silicon. This negative conclusion applies to room temperature properties while addition of cobalt has been proposed for high temperature applications [36]. This suggests extending the work done so far to high temperature.

Acknowledgements

The authors want to thank TQC Technologies for experimental support. This research did not receive any specific grant from funding agencies in the public, commercial or not-profit sectors.

References

[1] Jalava K, Soivio K, Laine J, et al. Elevated temperature thermal conductivities of some as-cast and austempered cast irons. Mater. Sci. Technol. 2018;34:327–333.

[2] Borsato T, Berto F, Ferro P, et al. Influence of solidification defects on the fatigue behavior of heavy-section silicon solution-stregthened ferritic ductile cast iron, Fatigue Fract. Eng. Mater. Struct. 2018;41:2231–2238.

[3] Yürektürk Y, Baydoğan M. Characterization of ferritic ductile iron subjected to successive aluminizing and austempering, Surf. Coat. Technol. 2018;347:142–149.

[4] Ikeda T, Noda N-A, Sano Y, Conditions for notch strength to be higher than static tensile strength in high-strength ductile iron, Eng. Fract. Mech. 2019;206:75–88

[5] Björkegren L-E, Hamberg K, Johannesson B. Mechanical properties and machinability of Si-solution-hardened ferritic ductile iron, AFS Trans. 1996;104:139–145.

[6] Björkegren L-E, Hamberg K. Silicon alloyed ductile iron with excellent ductility and machinability. Hilton Head Island, SC: Keith Millis Symposium on Ductile Cast Iron; 2003.

[7] Löblich H, Stets W. Werkstoff- und fertigungstechische Grundlagen der Herstellung und Anwendung von hoch siliciumhaltigem Gusseisen mit Kugelgraphit. Teil: 2. Impftechnologie, Abweichungen in der Graphiform, Bearbeitbarkeit. Giesserei 2013;100:42–53.

[8] Stets W, Löblich H, Gassner G, et al. Solution strengthened ferritic ductile cast iron properties, production and application, Int. J. Metalcast. 2014;8:35–40.

[9] Méndez S, Arenas MA, Niklas A, et al. Effect of silicon and graphite degeneration on high-temperature oxidation of ductile cast iron in open air, Oxid. Met. 2019;91:225–242.

[10] Arenas MA, Niklas A, Conde A, et al. Corrosion behaviour of ductile cast irons partially modified with silicon in 0.03 M NaCl, Rev. Met. 2014;50:e032.
[11] Reynaud A, Corrosion of cast irons (cap. 2). in: T.J.A. Richardson (Ed.). Shreir's Corrosion. vol. 3. Elsevier. Amsterdam. The Netherlands. 2010. p. 1737–1788.
[12] Jafar K-A, Behnam A-A. Influence of mold preheating and silicon content on microstructure and casting properties of ductile iron in permanent mold, J. Iron Steel Res. Int. 2011;18:34–39.
[13] Riebisch M, Seiler C, Pustal B, et al. Microstructure of as-cast high-silicon ductile iron produced via permanent mold casting, Int. J. Metalcast. 2019;3:112–120.
[14] González-Martínez R, de la Torre U, Ebel A, et al. Effects of high silicon contents on graphite morphology and room temperature mechanical properties of as-cast ferritic ductile cast irons. Part II – Mechanical properties, Mat. Sci. Eng. A 2018;712:803–811.
[15] González-Martínez R, de la Torre U, Lacaze J, et al. Effects of high silicon contents on graphite morphology and room temperature mechanical properties of as-cast ferritic ductile cast irons. Part I– Microstructure, Mat. Sci. Eng. A 2018;712:794–802.
[16] Franzen D, Weiß P, Pustal B, et al. Influence of aluminium on silicon microsegregation in solution strengthened ductile iron, Mater. Sci. Technol. 2019;35:687–694.
[17] Thury W, Hummer R, Nechtelberger E. Der Einfluss von Kobalt, Nickel un Kupfer auf das Gefüge und die mechanischen Eingenschaften von Gusseisen mit Kugelgraphit (in German). Giesserei-Praxis 1967;15:273–279.
[18] Mold EK. Kobaltlegiertes Gusseisen mit Kugelgraphit, Giesserei 1968;55:244–251.
[19] Hsu C-H, Chen M-L, Hu C-J. Microstructure and mechanical properties of 4% cobalt and nickel alloyed ductile irons, Mater. Sci. Eng. A 2007;444:339–346.
[20] Weiß P, Brachmann J, Bührig-Polaczek A, et al, Influence of nickel and cobalt on microstructure of silicon solution strengthened ductile iron, Mater. Sci. Technol. 2015;31:1479–1485.
[21] Duwe S, Tonn B, Ductile cast irons with high toughness at low temperatures, Mat. Sci. Forum 2018;925:334–341.
[22] Fischer SF, Brachmann J, Bührig-Polaczek A, et al. Metallurgische Verbesserung von mischkritallverfestigten Gusseisen mit Kugelgrafit Teil 2: Einfluss von Cobalt und Nickel auf die mechanischen Eigenschaften. (in German). Giesserei 2017;104:40–51.
[23] Castro M, Herrera M, Cisneros MM, et al. Simulation of thermal analysis applied to the description of the solidification of hypereutectic SG irons, Int. J. Cast Met. Res. 1999;11:369–374.
[24] Stefanescu DM, Lacaze J. Thermodynamics principles as applied to cast iron. in: ASM Handbook. vol 1A. Cast Iron Science and Technology. 2017. p. 31–45.
[25] Feret LR. Assoc. Internat. Pour I´Essai des Mat. Zurich. 2 Group D 1931.

[26] Zhou J, Schmitz W, Engler S. Untersuchung der gefügebildung von gusseisen mit kugelgraphit bei langsamer erstarrung. Giessereiforschung 1987;39:55–70.
[27] Prinz B, Eschborn KJ, Schulze T, et al. Untersuchung von ursachen von graphitentartungen bei gusseisen mit kugelgraphit in form von chunky-graphit, Giessereiforschung 1991;43:107–115.
[28] Sertucha J, Lacaze J, González-Martínez R, Chunky graphite in spheroidal graphite iron: review of recent results and definition of a predicting index, in ICASP5-CSSCR5, Salzburg, IOP Conf. Ser.: Mater. Sci. Eng. 2019;529:paper 012017.
[29] Bauer B, Pokopec IM, Petrič M, et al. Effect of Si and Ni addition on graphite morphology in heavy-section spheroidal graphite iron parts, Mat. Sci. Forum 2018;925:70–77.
[30] Gagné M, Labrecque, C, Javaid A, Effect of wall thickness on the graphite morphology and properties of D5-S austenitic ductile iron, AFS Trans. 2007;115:paper 07-005.
[31] Lacaze J, Larrañaga P, Asenjo I, et al. Influence of 1 wt% addition of Ni on structural and mechanical properties of ferritic ductile irons, Mater. Sci. Technol. 2012;28:603–608.
[32] de la Torre U, Loizaga A, Lacaze J, et al. As cast high silicon ductile irons with optimised mechanical properties and remarkable fatigue properties, Mater. Sci. Technol. 2014;30:1425–1431.
[33] Weiß P, Tekavčič A, Bührig-Polaczek A. Mechanistic approach to new design concepts for high silicon ductile iron, Mat. Sci. Eng. A 2018;713:67–74.
[34] Fukaya M, Miyazaki T, Kozakai T, Phase diagrams calculated for Fe-rich Fe-Si-Co and Fe-Si-Al ordering alloy systems, J. Mater. Sci. 1991;26:5420–5426.
[35] Raghavan V, Co-Fe-Si (cobalt-iron-silicon), J. Phase Equilibria, 1994;15:527–528.
[36] Janssen S, Sheng S. Gusseisen mit kobalt und bauteil und seine verwendung in dampfturbinen, EP-1808504A1, 2006.

Annex A

Literature data on the effect of cobalt on room temperature mechanical properties of ductile irons.

As mentioned in the introduction, four reports are available in the literature on the effect of cobalt on the room temperature mechanical properties of ferritic spheroidal graphite ductile irons. The papers by Thury et al. [17] and Mold [18] are old and deal with low silicon ductile irons, while more recent work at RWTH-Aachen [20, 22] deals with high silicon ductile irons. The two old papers were published in German, hence this annex which gives a short glance at the four of them.

Thury et al. [17] prepared near-eutectic ductile irons containing 2.06-2.24 wt.% Si and two others alloyed with 0.50 or 1.93 wt.% Co. The melts were cast in Y2 keel-blocks and were fully ferritic in the as-cast state. The relevant UTS, Y, A and HBW data are shown in table A1.

Table A1. UTS, YS, A and HBW values and C, Si and Co contents of the alloys investigated by Thury et al. [17].

Alloy	UTS (MPa)	YS (MPa)	A (%)	HBW	C (wt.%)	Si (wt.%)	Co (wt.%)
1	385	240	26.0	141	3.45-3.60	2.06-2.24	0.00
2	386	238	24.7	143	3.45-3.60	2.06-2.24	0.50
3	401	252	24.0	151	3.45-3.60	2.06-2.24	1.93

The work by Mold was much more extensive with additions of cobalt up to 15 wt.% with three ranges of silicon 1.6, 1.9 and 2.3 wt.%. The alloys were prepared in a high frequency induction furnace with 100 kg in capacity. Their cobalt content was adjusted by adding high purity element and the produced alloys were cast in Y keel-blocks though the authors did not give geometrical information. Some of the alloys were ferritised by heat-treating at 780°C for 5 h. For comparison purposes only data of fully ferritic structure in the as-cast state are showed in table A2.

Table A2. UTS, YS and A values and C, Si and Co contents of the fully ferritic alloys investigated by Mold [18].

Alloy	UTS (MPa)	YS (MPa)	A (%)	HBW	C (wt.%)	Si (wt.%)	Co (wt.%)
1	461	304	23.0	165	3.65	2.55	4.57
2	471	314	23.0	170	3.71	2.35	6.03

The works by Fischer et al. [22] and Weiss et al. [20] were carried out at RWTH-Aachen using the same procedures and indeed report the same results, Weiss et al. [20] published the microstructure results and Fischer et al. [22] the mechanical properties. The alloys contained 3.8-4.3 wt.% Si and

were alloyed with up to 4 wt.% Co. They were cast Y2 keel-blocks and showed a fully ferritic structure in the as-cast state.

Table A3. UTS, YS and A values, and Si and Co contents of the alloys investigated by Fischer et al. and Weiss et al. [22, 20].

Alloy	UTS (MPa)	YS (MPa)	A (%)	Si (wt.%)	Co (wt.%)
1	545	438	19.5	3.8	0
2	577	455	18.0	3.8	2
3	585	465	17.0	3.8	4
4	612	507	12.8	4.3	0
5	648	517	10.5	4.3	2
6	658	522	6.5	4.3	4